**Fabrication of reduced graphene oxide with high electrical conductivity by thermal-assisted photoreduction of electrochemically-exfoliated graphene oxide**

Yuji Hirotomi, Wataru Kubota, Toru Utsunomiya, Takashi Ichii, and Hiroyuki Sugimura

*Department of Materials Science and Engineering, Graduate School of Engineering, Kyoto University, Sakyo, Kyoto 606-8501, Japan*

E-mail: utsunomiya.toru.5v@kyoto-u.ac.jp

Abstract

Electrochemical exfoliation of graphite is a method for synthesizing graphene oxide (GO) with fewer structural defects than GO synthesized by conventional chemical oxidation. Photoreduction of GO has been focused due to their facile procedures, and environmental friendliness. In this report, electrochemically-exfoliated graphene oxide (EGO) was irradiated by vacuum ultraviolet (VUV) light at 140 ˚C under a high vacuum environment, named as thermal-assisted VUV light treatment. Conductive atomic force microscopy was used to investigate the electrical characteristics of individual sheets on the nanometer scale. The electrical conductivity of the treated sheet ($1.4\times10^5$ S $m^{-1}$) was higher than the pristine EGO by an order of magnitude. The chemical and structural analysis showed that the EGO was reduced and their π-conjugated domains were restored through a hybrid of photochemical and thermal treatment. These results indicate that our hybrid approach has the potential for reducing the EGO.

## 1. Introduction

Graphene, a two-dimensional single layer of covalently bonded carbon atoms with $sp^2$ hybridization arranged in a hexagonal lattice, is currently attracting attention in several applications due to its various interesting properties such as low friction[1], high electrical conductivity[2], mechanical strength[3], thermal conductivity[4]. Several methods for the synthesis of graphene have been developed, for instance, mechanical exfoliation[2], chemical vapor deposition (CVD)[5,6], epitaxial growth[7,8], and reduction of graphene oxide (GO)[9]. GO sheets consist of a graphitic carbon network bearing various types of oxygen-containing defects (hydroxyl, epoxide, carboxylic, and carbonyl)[10,11]. High-quality monolayer graphene can be produced by CVD or epitaxial growth[5]. In contrast, the reduction of GO is a low-cost method to create graphene-like materials, due to the easy bulk quantity production of GO. Reduced GO (rGO) with enhanced electrical conductivity can be utilized for further applications, such as sensors, flexible electronic devices, Li-ion batteries, and so on[12].

Currently, chemical and thermal reduction processes are frequently used in the reduction of GO [10,13–15]. However, hydrazine, a toxic reductant, is generally used in chemical reduction procedures[10], leading to environmental concerns. The high-temperature treatment for reducing GO is unsuitable for flexible electronics and also for some semiconductor processes, due to their thermal stability. On the other hand, photochemical reduction is a newly developed treatment to reduce GO[16–18]. According to the previous report, photon energy over 3.2 eV is needed during photochemical reduction and higher photon energy leads to the higher efficiency of reduction[16]. Our group also reported that GO chemically fabricated by modified Hummers' method (CGO) can be reduced by 172 nm vacuum ultraviolet (VUV) light irradiation in high vacuum ($<10^{-3}$ Pa) at room

temperature, as revealed by X-ray photoelectron spectroscopy (XPS)[19,20]. As 172 nm VUV light can transmit a commercially available quartz photomask, it is suitable for a light source of photo-patterning processes[21,22]. Photoreduction can draw conductive rGO patterns on GO sheets[23]. However, the electrical conductivity of the VUV-reduced GO measured by conductive atomic force microscopy (C-AFM) was approximately 0.2 S $m^{-1}$, which was much less than other rGO treated with other processes. It is necessary to develop an additional approach to improve the VUV photoreduction effect. By the observation of micro-Raman spectroscopy (μRS), it is clear that heating CGO at 140 ˚C changed the structure[24]. We will propose the reduction process of GO combining VUV light irradiation with heating at 140 ˚C, named as thermal-assisted VUV light treatment.

Recently, the exfoliation of graphite by anodization has been focused on as a novel synthesizing process of GO because of its environmental friendliness and potentially low cost[25–29]. When the positive voltage is applied to graphite in an aqueous electrolyte, oxygen functional groups are introduced by the reaction between graphite and ions or water molecules. After that, the oxidized graphite is exfoliated and monolayer or multilayers flakes of GO are produced by the gas pressure formed by intercalated species decomposition. This exfoliation process leads to the fast production of GO (less than 1 h). Additionally, electrochemically-exfoliated GO (EGO) has a larger size of the conjugated $\pi$-domains than CGO[30], which is beneficial for the production of high conductive rGO.

In this study, we will propose the combined method of reducing EGO with fewer defects than CGO, and demonstrate the relationship between electrical characteristics and structure of reduced EGO (rEGO) through C-AFM, XPS, and μRS. The heating at 140 ˚C during VUV irradiation is expected to enhance the recovery of graphene structure by repairing the lattice defects, as one combined reduction approach. Also, we use the EGO

as a precursor material for this thermal-assisted VUV light reduction. C-AFM holds great potential for the micro/nano electrical conductivity measurement of rGO[31–33], and we focus on the conductivity of individual sheets. The relationship between the $\pi$-conjugated structure and the electrical conductivity was considered from C-AFM analysis and μRS observation.

## 2. Experimental methods

### 2.1. Preparation of EGO

Electrochemically-exfoliated GO (EGO) was synthesized through the two-step electrochemical exfoliation process, concerning Cao's report[30]. Figure 1(a) shows the schematic illustration of electrochemical intercalation and oxidation setup. Galvanostatic charging was applied to graphite foil (99.8 %, 0.5 mm thickness, Alfa Aesar) in a two-electrode cell with concentrated sulfuric acid (97 %, Nacalai Tesque) and a platinum wire as an electrolyte and a cathode, respectively. The charging current was maintained at 100 mA for 20 min. For the next electrochemical step, the charged graphite foil was taken out from the first electrolyte, and potentiostatic charging was applied to the foil in a two-electrode cell with a platinum wire as a cathode and 0.1 M $(NH_4)_2SO_4$ (99 %, Fujifilm Wako Pure Chemical) aqueous solution as the electrolyte. Charging voltage was kept at 10 V and it took 10 min to complete the exfoliation of graphite flakes. Then exfoliated flakes were sonicated for 5 min and centrifuged at 13500 rpm for 10 min. After that, the supernatant was removed and N, N-dimethylformamide (DMF) was added. A set of steps from sonication to the addition of DMF was repeated 5 times to replace the original solvent, which is a mixture of water and $(NH_4)_2SO_4$, with DMF. The dispersion was maintained for 24 h to precipitate and remove any aggregations, as shown in Fig. 1(b).

## 2.2. Reduction of EGO by thermal-assisted VUV light irradiation

EGO dispersed in DMF was spin-coated onto the Si substrates. The sample was transferred into a highly evacuated chamber ($<10^{-3}$ Pa). The sample stage in the chamber was heated to 140 $^{o}$C and then the samples were irradiated by VUV light (center wavelength of 172 nm, 9.5 mW cm$^{-2}$, Ushio) at a 10 mm distance from the window to the substrate surface, as schematically shown in Fig. 1(c).

## 2.3. Characterization

The highly doped p-type Si substrates with a thickness of 90 nm $SiO_2$ were used as the substrate for the structural analysis and AFM measurements. The chemical condition and structure of each GO and rGO sheet were characterized by micro-Raman spectroscopy (μRS, Lucir) and x-ray photoelectron spectroscopy (XPS, ESCA-3400, Shimadzu). In XPS measurements, an Mg target was used as an x-ray source, with an accelerating voltage and current of 10 kV and 10 mA, respectively. μRS observation was carried out using a 532 nm laser as the excitation source. MFP-3D (Oxford Instruments) was used for AFM and C-AFM measurements under ambient conditions. We used Rh-coated Si cantilevers (SI-DF3-R, spring const. 1.6 N m$^{-1}$, Hitachi High-Tech) for the simultaneous measurement of electrical conductivity with topography in contact mode. Al-backside-coated Si cantilevers (SI-DF-40, spring const. 35 N m$^{-1}$, Hitachi High-Tech) were used for amplitude modulation AFM topographic imaging. The highly doped p-type Si substrates with a thickness of 300 nm $SiO_2$ were used as the substrate for C-AFM measurements. During C-AFM measurements, the tip load was kept at 32 nN and a constant voltage of -1 V was applied to the cantilever. As shown in Fig. 1(d), Au/Ti film was deposited on a part of the GO-coated substrate to connect the sheet with the electrode (100 nm Au film with 10 nm Ti adhesion layer).

## 3. Results and Discussion

Figure 1(b) shows the solution including EGO in DMF after sonication. The supernatant showed a dark brown color and was untransparent. This proposes that monolayer and multilayer EGO sheets were dispersed. AFM was used to investigate the topography and thickness of EGO sheets before and after VUV light irradiation and/or heating under a high vacuum environment. We will use notations for samples after treatments in the following parts. “EGO-VUV-140” expresses the EGO sample after VUV light irradiation at 140 ℃ in a high vacuum environment. “EGO-VUV-RT” and “EGO-dark-140” mean the EGO samples after VUV light irradiation at room temperature, and after heating at 140 ˚C without VUV light irradiation, respectively. Figure 2(a) shows an AFM image of the pristine EGO sheets deposited on the thermally grown $SiO_2$ substrate. The size and thickness of the pristine EGO sheets were 2~5 μm and 1.0~1.2 nm, respectively. Some regions of the sheets are deposited as a monolayer sheet, and the other areas as multilayer with a thickness of over 2 nm because of the bending of a monolayer sheet or the overlapping of multiple sheets. On the contrary, thicknesses of EGO-VUV-RT, EGO-dark-140, and EGO-VUV-140 were all 0.8~1.0 nm (Figs. 2(b-d)). This means that each treatment leads to the decrease of the thickness of the EGO monolayer. Monolayer graphene has a thickness of 0.35 nm, so thicknesses of the EGO after each treatment were still larger than graphene[34]. It is reported that the thickness of CGO decreases by photochemical reaction or the thermal process with microwave[35,36]. Our results agreed with the literature in terms of declining the thickness.

XPS analysis gives us information about chemical conditions and oxygen functional groups on each sample. Figure 3 shows the XPS C1s spectra of the pristine EGO and EGO after each treatment. Here, the spectra were calibrated to the Si 2p peak at 103.5 eV

derived from the Si-O bond and normalized by the peak intensity at ~284 eV. According to the previous report[34], the binding energies of C=C/C-C in the benzene ring, C-O and $sp^3$ C-C, C=O in unreduced GO are approximately 284.6, 286.6, 287.9 eV, respectively. Based on this, the spectra in Fig. 3 were deconvoluted to 3 peaks, i.e. $sp^2$ graphitic C=C, C-O, and C=O. From the peak fitting result, mainly oxygen functional groups included in EGO are considered hydroxyl and epoxy. The ratio of oxygen to carbon ($R_{O/C}$) on EGO, which was derived from the areas of each peak component, was estimated to be ~0.40. Similarly, $R_{O/C}$ on EGO-VUV-RT, EGO-dark-140, EGO-VUV-140 were calculated as ~0.27, ~0.35, and ~0.30, respectively. The decrease of $R_{O/C}$ by each treatment indicates that either heating at 140 ˚C or VUV light irradiation causes the reduction of EGO. In addition, VUV light irradiation for 64 minutes is more effective for the reduction of EGO than heating at 140 ˚C. However, $R_{O/C}$ on EGO-VUV-RT was slightly larger than that on EGO-VUV-140. Therefore, thermal-assisted VUV light treatment doesn't lead to the additional dissociation of oxygen on EGO. This removal of oxygen functional groups leads to the reduced thickness of the sheets, as observed by AFM (Fig. 2).

Raman spectroscopy can detect the extent of graphitic domains. Figure 4 shows the 532 nm micro-Raman spectra of the pristine EGO and EGO after each treatment. We will use notation *I* for peak height. For example, *I*(G) expresses the height of the G peak. Additionally, *I*(D)/*I*(G), *I*(D')/*I*(G), and *I*(2D)/*I*(G) express the height of D, D', and 2D peaks based on that of the G peak, respectively. The spectra shown in Fig. 4 display the carbon D, G, D', and 2D band peaks at ~1350, ~1580, ~1610, and ~2700 $cm^{-1}$, respectively. We observed obvious splitting of the G and the D' peak in Fig. 4 (b-d). *I*(D)/*I*(G) of EGO-VUV-RT (~2.4) was larger than that of the pristine EGO (~0.8). Also, *I*(D)/*I*(G) of EGO-dark-140 (~1.4) was larger than that of pristine EGO but smaller than EGO-VUV-RT. According to the previous report[37], when the average distance between

defects ($L_D$) on highly oriented pyrolytic graphite is less than 5 nm, $I$(D)/$I$(G) increases and D' peak appears as $L_D$ increases. Therefore, our results indicate that $sp^2$ conjugated hexagonal carbon frameworks on EGO were restored by VUV light irradiation or heating at 140 ˚C. $I$(2D)/$I$(G) of EGO-VUV-RT (~0.5) was larger than that of the pristine EGO (~0.2). Moreover, $I$(2D)/$I$(G) of EGO-VUV-140 (~1.0) was larger than that of EGO-VUV-RT. This feature shows the increase of graphitic domains in the sheets[38]. $I$(D)/$I$(G) of EGO-VUV-140 (~2.1) was slightly smaller than that of EGO-VUV-RT (~2.4). Also, $I$(D')/$I$(G) of EGO-VUV-140 (~0.4) was slightly smaller than that of EGO-VUV-RT (~0.6). When $L_D$ is over 4 nm, $I$(D)/$I$(G) and $I$(D')/$I$(G) decrease as $L_D$ increases[37]. Therefore, due to the heating at 140 ˚C during VUV light irradiation, the additional restoration of $sp^2$ conjugated domains occurred. Additionally, it is possible that $L_D$ of EGO-VUV-140 is over 4 nm. This means that the combination of VUV light irradiation and heating under a high vacuum effectively reduce EGO sheets. Although there was some variability in micro-Raman spectra of each sheet, possibly due to the inhomogeneous structure of EGO after each treatment, the restoration of the EGO has taken place without supplying the carbon sources during this combined treatment. The obtained structural and chemical properties of EGO-VUV-140 can be correlated with electrical conductivities.

The nano-scaled electrical conductivity of EGO-VUV-140 was measured by C-AFM in contact mode AFM. We obtained the C-AFM image including the boundary of the EGO-VUV-140 sheet and the electrode connected to the sheet as shown in Fig. 5(a, b). This configuration can detect the electrical characteristics in the in-plane direction of the individual sheet. The region of the deposited electrode (100 nm Au film with 10 nm Ti adhesion layer) corresponds to the white area in the upper side of Fig. 5(b), and the black area in the lower side corresponds to the $SiO_2$ substrate. While thermally grown $SiO_2$

substrate with a thickness of 300 nm showed insulation, the EGO-VUV-140 monolayer sheet connected to the electrode had electrical conductivity to some extent as shown in the grey zone of Fig. 5(b). In the sheet, the current decreased as the distance from the electrode increased due to the integrated resistivity of the EGO-VUV-140 sheet. The inhomogeneous electrical conductivity on the EGO-VUV-140 sheet can reflect domain features such as $sp^2$ graphitic domains or $sp^3$ oxidized domains. When the tip is located on a carbon hexagonal domain, current flows through a conductive path from the spot of the tip to the electrode, leading to a high current signal. At the same time, when the tip is on a low conductive domain, the lower current signal is detected. This difference resulted in the variation of the measured current in the EGO-VUV-140 sheet and the formation of high/low conductive domains. While the high conductive domains may be similar to graphene structure, low conductive domains are derived from some defective structures of the EGO-VUV-140 sheet. As shown in Figs. 3 and 4, EGO-VUV-140 has defects, that is, carbon structure with oxygen functional groups or non-hexagonal bonding. These defects were perhaps formed in the process of synthesis of EGO or during VUV light irradiation. This should have caused the local existence of low conductive domains, leading to the variation of the electrical conductivity.

Figures 5(c) and 5(d) show the current profile and corresponding resistance profile along the red line in Fig. 5(b). The resistance was converted from the current using Ohm's law. The measured current along the line varied linearly except for points of defects so that it became smaller as the distance from the electrode increased. Following the previous report[39], this means that current detours around defects. Here, we regarded as the electrical path, the triangle region on the EGO-VUV-140 sheet formed by the tip, and the electrode side connected with the sheet. Therefore, electrical conductivity can be

calculated by following formulas. At first, the resistance of the micro area shown as the trapezoid in Fig. 5(e) is given by

$$dR = \rho \frac{dl}{\left\{\frac{l}{L}(W_e - W_t) + W_t\right\} T}, \quad (1)$$

where $\rho$ is the resistivity of the EGO-VUV-140 sheet, $l$ is the distance between the tip and the trapezoid area, $L$ is the distance between the tip and the electrode, $T$ is the thickness of the sheet, $W_e$ is the connected length of the sheet and the electrode, and $W_t$ is the diameter of the area between the tip and the surface of the sheet. Next, following the Hertzian contact mechanics model, we calculated $W_t$ to be 2.3 nm from the tip contact area. The value of the tip contact area $A$ was calculated as 4.2 nm$^2$ by

$$A = \pi \left( \frac{r_{tip} \cdot F_{load}}{K} \right)^{\frac{2}{3}}, \quad (2)$$

where $r_{tip}$ is the radius of the tip, $F_{load}$ is the force applied between the sample and the tip, and $K$ is the elastic modulus of the sample. Finally, the value of the electrical conductivity $\sigma$ of the sheet was calculated by integrating the Eq. (1), that is

$$\sigma = \frac{1}{\rho} = \frac{L}{R} \frac{1}{T(W_e - W_t)} \ln\left(\frac{W_e}{W_t}\right). \quad (3)$$

The calculated electrical conductivity of the EGO-VUV-140 was about 140000 S m$^{-1}$ by determining the experimental parameters of $W_e$ as 5.7 μm and $T$ as 0.9 nm. In the previous report, the electrical conductivity of pristine EGO was calculated to be 27000 S m$^{-1}$[39]. Through VUV light treatment at 140 ˚C, the electrical conductivity of EGO was enhanced by an order of magnitude, which means that the conductive path increased in the in-plane direction on the EGO-VUV-140 sheet. Moreover, the sheet resistance of GO reduced by heating in the presence of EtOH was reported to be around 10 kΩ sq$^{-1}$[40]. As the electrical conductivity of the EGO-VUV-140 was converted to around 7.1 kΩ sq$^{-1}$ in this result, this value was the same order as the previous report.

Considering the results in Figs. 3-5 comprehensively, we will propose the possible structural changes of EGO due to VUV light irradiation in high vacuum environments with heating at 140 ˚C. Mainly the electrical conductivity of EGO is derived from conjugated π-domains, so the restoration of π-domains by VUV light treatment at 140 ˚C caused the high electrical conductivity. As Smirnov pointed out, the model of photochemical reduction is different from that of thermal reduction[24,41]. In the photochemical reduction process, π-domains of significant sizes appear only when the mobility of GO nanosheet fragments is possible. On the other hand, in the thermal reduction process, remote carbon hexagonal domains are connected. In this study, the restoration of $sp^2$ graphitic domains due to the phenomenon similar to these two ways may occur simultaneously by VUV light irradiation at 140 ˚C. This hypothesis satisfies not only the high electrical conductivity but also the results of XPS and μRS. Due to the dissociation of oxygen functional groups and the restoration of $sp^2$ graphitic domains, the electrical conductivity of the EGO-VUV-140 was higher than the pristine EGO.

## 4. Conclusions

We proposed the combined reduction process to fabricate rEGO with high electrical conductivity. C-AFM was used to investigate the electrical characteristics of the EGO-VUV-140 monolayer sheet on the nanometer scale. The electrical conductivity of the EGO-VUV-140 was calculated to be about 140000 S $m^{-1}$. Larger electrical conductivity of the EGO-VUV-140 than that of the pristine EGO in the previous report[39] by an order of magnitude was proved. Additionally, μRS observations show that this thermal-assisted VUV light treatment changes the structure of the pristine EGO more than only heating or VUV light irradiation under the high vacuum condition. Combining C-AFM measurements with XPS and μRS analysis, it can be proposed that the dissociation of

oxygen functional groups and the restoration of $sp^2$ conjugated graphitic domains by VUV light irradiation with heating at 140 ˚C leads to the high electrical conductivity of the EGO-VUV-140. Our study shows that the combination of VUV light irradiation and heating is significantly effective for the reduction of EGO sheets.

## Acknowledgements

This work was partially supported by JSPS KAKENHI grants JP18K18946, JP20H02450, and JP20J20411; and the Murata Science Foundation.

## References

[1] C. Lee, Q. Li, W. Kalb, X.Z. Liu, H. Berger, R.W. Carpick, and J. Hone, *Science,* **328**, 76 (2010).

[2] K.S. Novoselov, A.K. Geim, S. V. Morozov, D. Jiang, Y. Zhang, S. V. Dubonos, I. V. Grigorieva, and A.A. Firsov, *Science,* **306**, 666 (2016).

[3] C. Lee, X. Wei, J.W. Kysar, and J. Hone, *Science,* **321**, 385 (2008).

[4] S. Ghosh, I. Calizo, D. Teweldebrhan, E.P. Pokatilov, D.L. Nika, A.A. Balandin, W. Bao, F. Miao, and C.N. Lau, *Appl. Phys. Lett.*, **92**, 1 (2008).

[5] X. Li, W. Cai, J. An, S. Kim, J. Nah, D. Yang, R. Piner, A. Velamakanni, I. Jung, E. Tutuc, S.K. Banerjee, L. Colombo, and R.S. Ruoff, *Science,* **324**, 1312 (2009).

[6] G. Deokar, J. Avila, I. Razado-Colambo, J.L. Codron, C. Boyaval, E. Galopin, M.C. Asensio, and D. Vignaud, *Carbon N. Y.*, **89**, 82 (2015).

[7] C. Berger, Z. Song, X. Li, X. Wu, N. Brown, C. Naud, D. Mayou, T. Li, J. Hass, A.N. Marchenkov, E.H. Conrad, P.N. First, and W.A. de Heer, *Science,* **312**, 1191 (2006).

[8] C. Berger, Z. Song, T. Li, X. Li, A.Y. Ogbazghi, R. Feng, Z. Dai, N. Alexei, M.E.H. Conrad, P.N. First, and W.A. De Heer, *J. Phys. Chem. B*, **108**, 19912 (2004).

[9] S. Stankovich, D.A. Dikin, R.D. Piner, K.A. Kohlhaas, A. Kleinhammes, Y. Jia, Y. Wu, S.B.T. Nguyen, and R.S. Ruoff, *Carbon N. Y.*, **45**, 1558 (2007).

[10] S. Park and R.S. Ruoff, *Nat. Nanotechnol.*, **4**, 217 (2009).

[11] M.J. Allen, V.C. Tung, and R.B. Kaner, *Chem. Rev.*, **110**, 132 (2010).

[12] S. Pei and H.M. Cheng, *Carbon N. Y.*, **50**, 3210 (2012).

[13] D.R. Dreyer, S. Park, C.W. Bielawski, and R.S. Ruoff, *Chem. Soc. Rev.*, **39**, 228 (2010).

[14] Y. Zhu, S. Murali, W. Cai, X. Li, J.W. Suk, J.R. Potts, and R.S. Ruoff, *Adv. Mater.*, **22**, 3906 (2010).

[15] H. Bai, C. Li, and G. Shi, *Adv. Mater.*, **23**, 1089 (2011).

[16] V.A. Smirnov, A.A. Arbuzov, Y.M. Shul'ga, S.A. Baskakov, V.M. Martynenko, V.E. Muradyan, and E.I. Kresova, *High Energy Chem.*, **45**, 57 (2011).

[17] X.H. Tai, S.W. Chook, C.W. Lai, K.M. Lee, T.C.K. Yang, S. Chong, and J.C. Juan, *RSC Adv.*, **9**, 18076 (2019).

[18] R.Y.N. Gengler, D.S. Badali, D. Zhang, K. Dimos, K. Spyrou, D. Gournis, and R.J.D. Miller, *Nat. Commun.*, **4**, 1 (2013).

[19] Y. Tu, T. Utsunomiya, T. Ichii, and H. Sugimura, *J. Vac. Sci. Technol. B, Nanotechnol. Microelectron. Mater. Process. Meas. Phenom.*, **35**, 03D110 (2017).

[20] Y. Tu, T. Ichii, T. Utsunomiya, and H. Sugimura, *Appl. Phys. Lett.*, **106**, 133105 (2015).

[21] A. Schreiber, B. Kühn, E. Arnold, F.J. Schilling, and H.D. Witzke, *J. Phys. D. Appl. Phys.*, **38**, 3242 (2005).

[22] A.I.A. Soliman, Y. Tu, T. Utsunomiya, T. Ichii, and H. Sugimura, *Langmuir*, **33**, 10829 (2017).

[23] Y. Tu, H. Nakamoto, T. Ichii, T. Utsunomiya, O.P. Khatri, and H. Sugimura, *Carbon N. Y.*, **119**, 82 (2017).

[24] V.A. Smirnov, Y.M. Shul'ga, N.N. Denisov, E.I. Kresova, and N.Y. Shul'ga, *Nanotechnologies Russ.*, **7**, 156 (2012).

[25] J. Ren, X. Zheng, Z. Tian, D. Li, P. Wang, and B. Jia, *Appl. Phys. Lett.*, **109**, (2016).

[26] P. Yu, Z. Tian, S.E. Lowe, J. Song, Z. Ma, X. Wang, Z.J. Han, Q. Bao, G.P. Simon, D. Li, and Y.L. Zhong, *Chem. Mater.*, **28**, 8429 (2016).

[27] B. Gurzęda, P. Florczak, M. Kempiński, B. Peplińska, P. Krawczyk, and S. Jurga, *Carbon N. Y.*, **100**, 540 (2016).

[28] A. Ambrosi and M. Pumera, *Chem. Eur. J.*, **22**, 153 (2016).

[29] A.M. Abdelkader, H. V. Patten, Z. Li, Y. Chen, and I.A. Kinloch, *Nanoscale*, **7**, 11386 (2015).

[30] J. Cao, P. He, M.A. Mohammed, X. Zhao, R.J. Young, B. Derby, I.A. Kinloch, and R.A.W. Dryfe, *J. Am. Chem. Soc.*, **139**, 17446 (2017).

[31] Y. Tu, T. Utsunomiya, S. Kokufu, M. Soga, T. Ichii, and H. Sugimura, *Langmuir*, **33**, 10765 (2017).

[32] S. Lim, H. Park, G. Yamamoto, C. Lee, and J.W. Suk, *Nanomaterials*, **11**, 2575 (2021).

[33] J.M. Mativetsky, E. Treossi, E. Orgiu, M. Melucci, G.P. Veronese, P. Samorì, and V. Palermo, *J. Am. Chem. Soc.*, **132**, 14130 (2010).

[34] J.I. Paredes, S. Villar-Rodil, P. Solís-Fernández, A. Martínez-Alonso, and J.M.D. Tascón, *Langmuir*, **25**, 5957 (2009).

[35] W. Chen, L. Yan, and P.R. Bangal, *Carbon N. Y.*, **48**, 1146 (2010).

[36] Y. Matsumoto, M. Koinuma, S. Ida, S. Hayami, T. Taniguchi, K. Hatakeyama, H. Tateishi, Y. Watanabe, and S. Amano, *J. Phys. Chem. C*, **115**, 19280 (2011).

[37] M.M. Lucchese, F. Stavale, E.H.M. Ferreira, C. Vilani, M.V.O. Moutinho, R.B. Capaz, C.A. Achete, and A. Jorio, *Carbon N. Y.*, **48**, 1592 (2010).

[38] L.G. Cançado, A. Jorio, E.H.M. Ferreira, F. Stavale, C.A. Achete, R.B. Capaz, M.V.O. Moutinho, A. Lombardo, T.S. Kulmala, and A.C. Ferrari, *Nano Lett.*, **11**, 3190 (2011).

[39] W. Kubota, T. Utsunomiya, T. Ichii, and H. Sugimura, *Jpn. J. Appl. Phys.*, **59**, SN1001 (2020).

[40] K. Kanishka, H. De Silva, H.-H. Huang, S. Suzuki, and M. Yoshimura, *Jpn. J. Appl. Phys.*, **58**, SIIB07 (2019).

[41] C. Mattevi, G. Eda, S. Agnoli, S. Miller, K.A. Mkhoyan, O. Celik, D. Mastrogiovanni, G. Granozzi, E. Carfunkel, and M. Chhowalla, *Adv. Funct. Mater.*, **19**, 2577 (2009).

## Figure Captions

**Fig. 1.** (a) Schematic illustration of electrochemical exfoliation. (b) The photograph of EGO dispersed in DMF after sonication. Schematic illustration of (c) the thermal-assisted VUV light treatment, and (d) the C-AFM measurement.

**Fig. 2.** AFM topographical images and corresponding height profiles measured on (a) pristine EGO, (b) EGO-VUV-RT, (c) EGO-dark-140, and (d) EGO-VUV-140. Height profiles were along the red lines in the corresponding topographical images.

**Fig. 3.** XPS C 1s spectra of (a) pristine EGO, (b) EGO-VUV-RT, (c) EGO-dark-140, and (d) EGO-VUV-140. Peak intensity was normalized by C-C peak at approximately 284 eV.

**Fig. 4.** Raman spectra of (a, e) pristine EGO, (b, f) EGO-VUV-RT, (c, g) EGO-dark-140, and (d, h) EGO-VUV-140. (a-d) high-resolution G and D band regions, and (e-h) whole spectra including 2D regions.

**Fig. 5.** Contact-mode AFM images for the (a) topography and (b) current. (c) The current and (d) the resistance profiles along the red line in the current mapping image. (e) Schematic illustration of C-AFM measurement for calculating the electrical conductivity of the EGO-VUV-140 sheet.

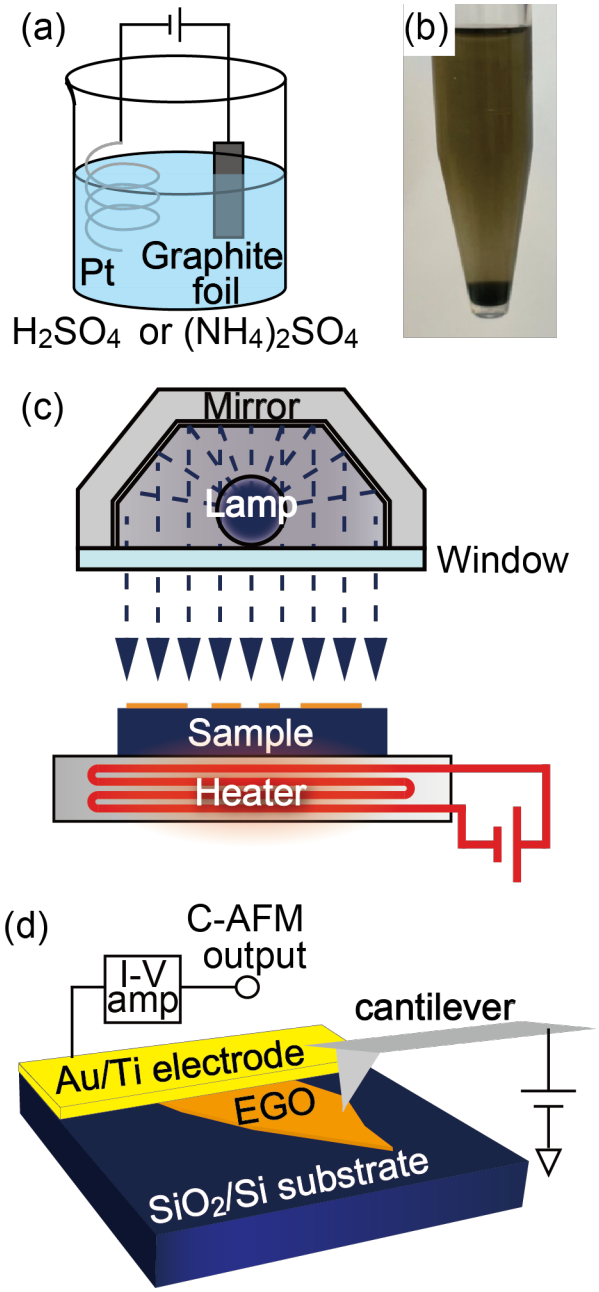
(a)
Pt
Graphite foil
H2SO4 or (NH4)2SO4
(b)
(c)
Mirror
Lamp
Window
Sample
Heater
(d)
C-AFM output
I-V amp
cantilever
Au/Ti electrode
EGO
SiO2/Si substrate

Fig. 1.

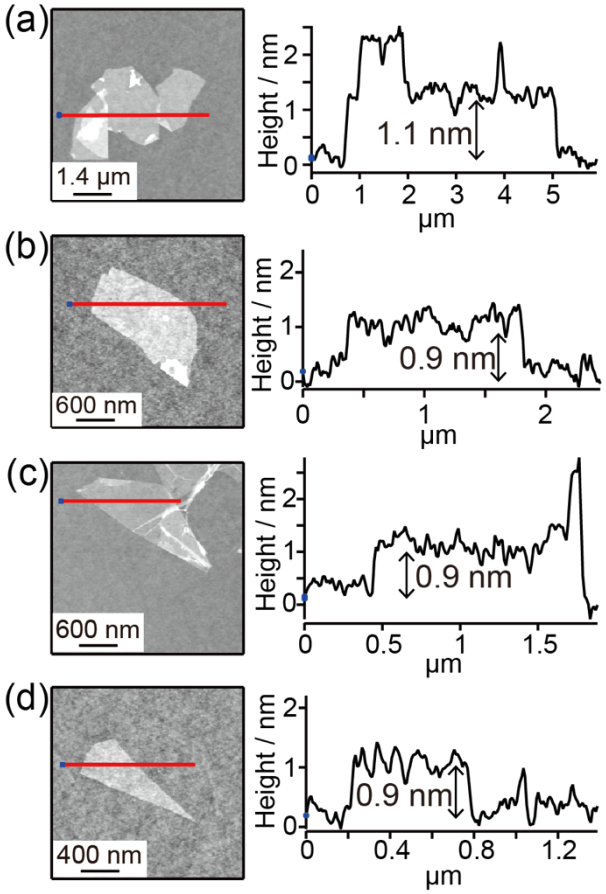
(a)
1.4 μm
Height / nm
1.1 nm
μm
(b)
600 nm
Height / nm
0.9 nm
μm
(c)
600 nm
Height / nm
0.9 nm
μm
(d)
400 nm
Height / nm
0.9 nm
μm

Fig. 2.

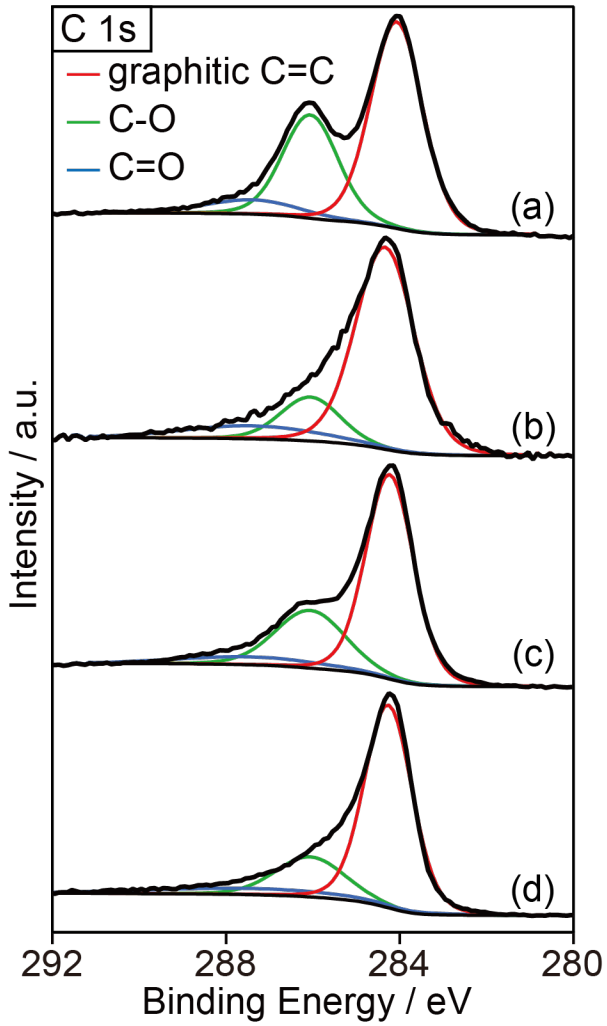
C 1s
graphitic C=C
C-O
C=O
(a)
(b)
(c)
(d)
Intensity / a.u.
292
288
284
280
Binding Energy / eV

Fig. 3.

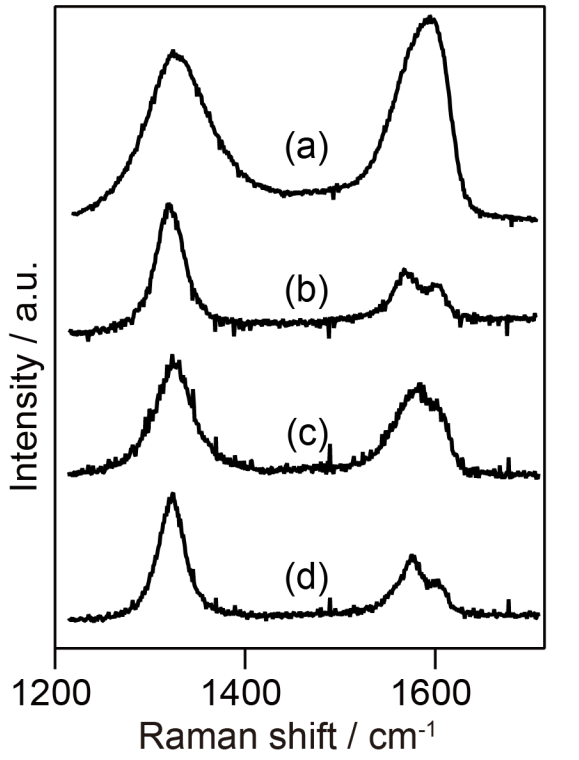
(a)
(b)
(c)
(d)
Intensity / a.u.
1200
1400
1600
Raman shift / cm-1

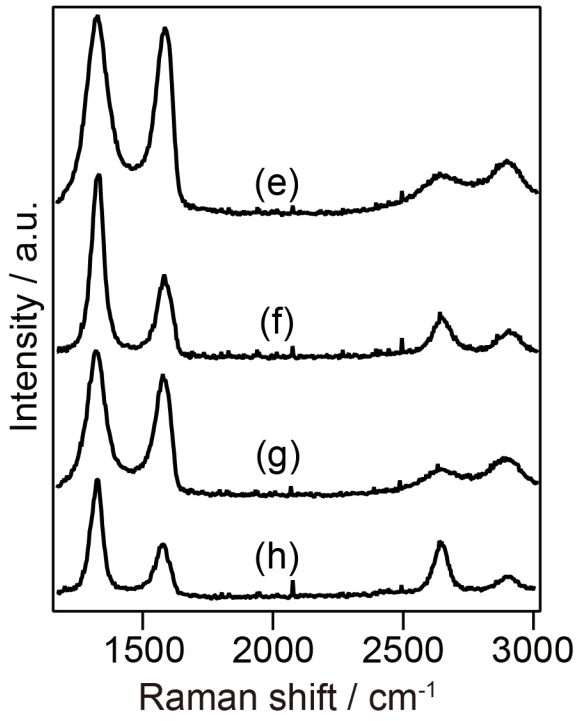
(e)
(f)
(g)
(h)
Intensity / a.u.
1500
2000
2500
3000
Raman shift / cm-1

Fig. 4.

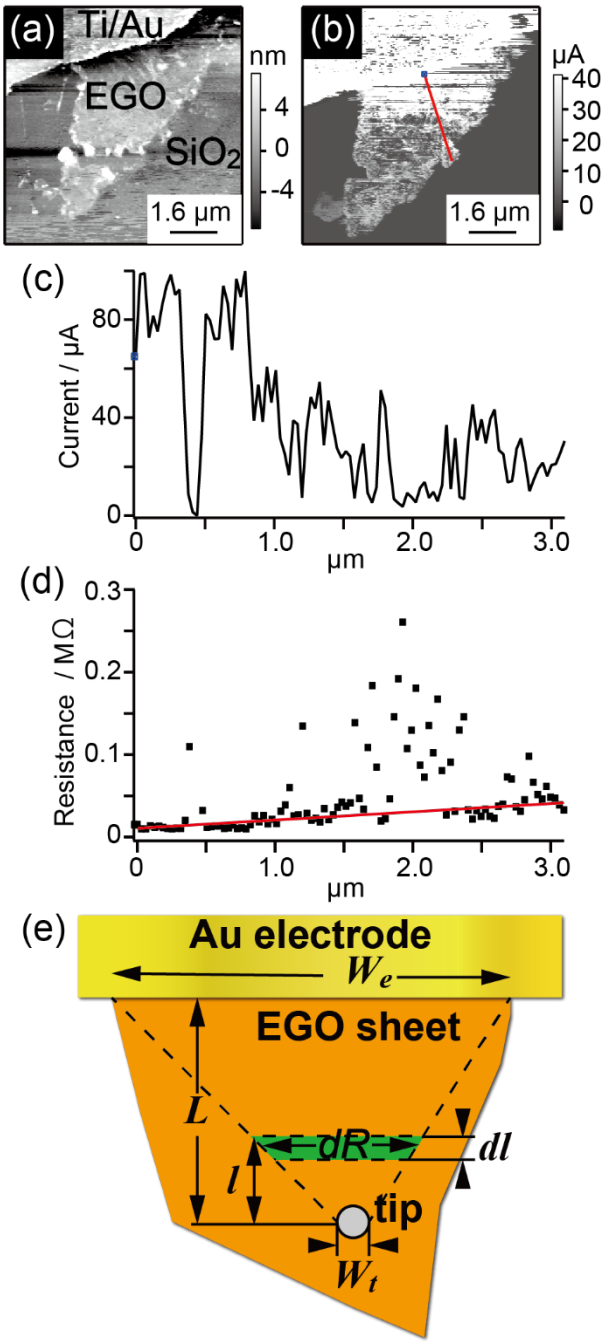
(a)
Ti/Au
EGO
SiO2
1.6 μm
nm
4
0
-4
(b)
1.6 μm
μA
40
30
20
10
0
(c)
Current / μA
80
40
0
0
1.0
2.0
3.0
μm
(d)
Resistance / MΩ
0.3
0.2
0.1
0
0
1.0
2.0
3.0
μm
(e)
Au electrode
We
EGO sheet
L
dR
dl
l
tip
Wt

Fig. 5.